

# Bidirectional-Resistant Ductile End Diaphragms with Buckling Restrained Braces for Skewed Steel Bridges



**O.C. Celik**

*Istanbul Technical University, Faculty of Architecture, Istanbul, 34437, Turkey*

**M. Bruneau**

*University at Buffalo, Department of CSEE, Buffalo, NY, 14260, USA*

## **SUMMARY:**

To reduce seismic demands in existing and new steel bridges, several seismic energy dissipation devices (including seismic isolators) have previously been proposed. For the seismic protection of steel bridges, specially designed ductile end diaphragms have proved to dissipate seismic input energy in regular (i.e. nonskewed) bridges. Since many bridges are built on a skew and AASHTO (2009) provides no guidance on how to implement ductile diaphragms in skewed bridges, two bidirectional end diaphragm configurations (EDS-1 and EDS-2) with buckling restrained braces (BRBs) are proposed and numerically investigated. To assess the relative effectiveness of the proposed systems, closed-form solutions are developed using nondimensional bridge geometric ratios. Numerical results indicate that skewness more severely affects end diaphragm behavior when  $\varphi \geq 30^\circ$ . Comparisons reveal that although both end diaphragm systems can be used with confidence as ductile seismic fuses, each system has advantages that may favor its implementation, depending on project-specific constraints.

*Keywords: Skewed steel bridges, end diaphragms, seismic retrofit, buckling restrained braces (BRBs)*

## **1. INTRODUCTION**

Buckling restrained braces (BRBs) have recently been implemented in buildings as seismic energy dissipation members, mostly in Japan and in the United States. Because of their stable, unpinched hysteretic characteristics and ease of design, the rate of implementation in building applications is increasing worldwide. BRBs have also been used to retrofit the Minato Bridge in Japan (Kanaji et al. 2003). Since many slab-on-girder and deck-truss bridges in North America were built without seismic design considerations, they may suffer damage in future earthquakes. The end diaphragms in these bridges generally do not have ductile details (both members and connections). To reduce seismic demands in existing and new steel bridges, bidirectional-resistant ductile end diaphragms with BRBs are proposed in this work.

Previous studies (e.g., Zahrai and Bruneau 1999a,b; Carden et al. 2006; Celik and Bruneau 2007) support that significant energy can be dissipated in ductile bridge end diaphragms, while reducing seismic demands in other substructure and superstructure bridge elements. Past research on end diaphragms has shown how shear panel systems (SPS), steel triangular plate added damping and stiffness devices (TADAS), eccentrically braced end diaphragms (EBF), and buckling restrained braces (BRBs) could be detailed to provide an appropriate seismic performance.

Currently, ductile diaphragms have to be combined with other lateral load resisting strategies to address seismic excitations along the bridge's longitudinal axis. Also, AASHTO (2009) provides no guidance on how to implement ductile diaphragms in skewed bridges—even though steel bridges with skewed superstructure geometries are commonly encountered at highway interchanges, river crossings, and other places because of alignment limitations. To address this need and to resolve some shortcomings of the known end diaphragm systems (i.e. end diaphragms incorporating SPS, TADAS,

or EBF), two bidirectional end diaphragm configurations, namely, EDS-1 and EDS-2, with BRBs are proposed and numerically investigated. Bidirectional end diaphragm is a new concept, and can be implemented both in straight and skewed steel bridge superstructures to resist bidirectional earthquake effects. Although they are considered here in the perspective of new bridge design, the information presented is also applicable to existing steel bridges for seismic retrofit purposes.

## 2. DUCTILE END DIAPHRAGM CONFIGURATIONS FOR SKEWED BRIDGES

Two types of ductile end diaphragm bracing configurations as seismic fuses are considered in this work:

End Diaphragm System-1 (EDS-1): Two pairs of BRBs are installed at each end of a span, in a configuration that coincides with the skew and longitudinal directions (Fig. 1a).

End Diaphragm System-2 (EDS-2): A single pair of BRBs is installed at each end of a span, at an angle that does not coincide with the bridge longitudinal and skew directions (Fig. 1b).

In EDS-1, the bottom connection of the pair of BRBs oriented in the skew direction can be connected either to the abutment or between web stiffeners of the bridge girders. The pair of longitudinal BRBs is a new concept and needs to be connected either to the horizontal (next to the bearings) or the vertical face of the abutments – as would be the BRBs in EDS-2. The BRBs connecting to the abutment need to be in series with lock-up devices that allow thermal expansion under normal conditions, but engage the BRBs during earthquakes. For the deck level connection, specially designed cross beams are required to elastically resist forces from the BRBs, unless connection to the existing interior cross frames or girders is developed without damaging any internal component (capacity design). Note that, since significant forces may develop in the BRBs, all components to which the BRBs connect should be checked to ensure that they are able to resisting such forces without yielding and without undesirable deformations. Details that do not induce large moments at the BRB's ends may be also desirable. Examples of such BRB connections are available in Lopez and Sabelli (2004).

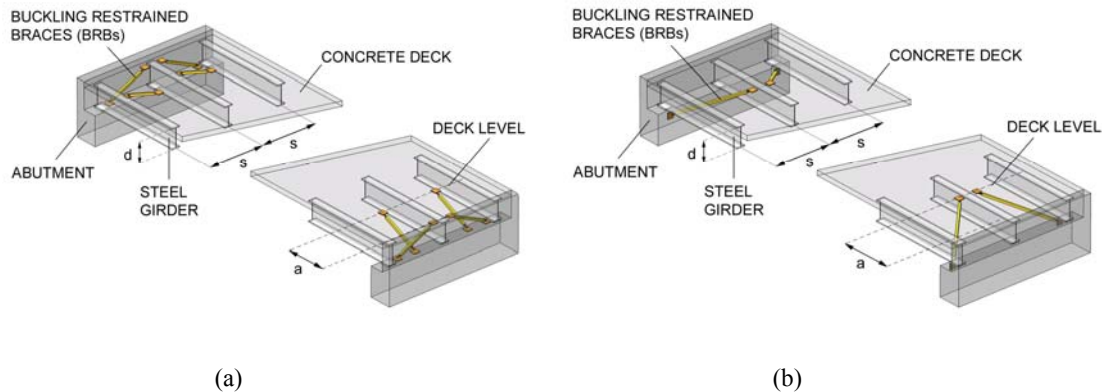


**Figure 1.** Ductile end diaphragm configurations for slab-on-girder steel bridges (a) EDS-1 (b) EDS-2 (intermediate cross-frames not shown for clarity)

## 3. ASSUMPTIONS AND SIMPLIFIED 3D MODELING

As shown in Fig. 2, an ideal elastic-plastic hysteretic model with equal tension and compression capacities ( $T_y=C_y$ ) is used for the BRBs. Furthermore, the BRBs are assumed to have pinned end connections and are not active under gravity loading. Cross sectional areas of BRBs and skew angles are taken to be the same for each of the two end diaphragms. It is further considered that the rigid concrete deck and the steel girders are continuously connected (i.e. composite girders), but are

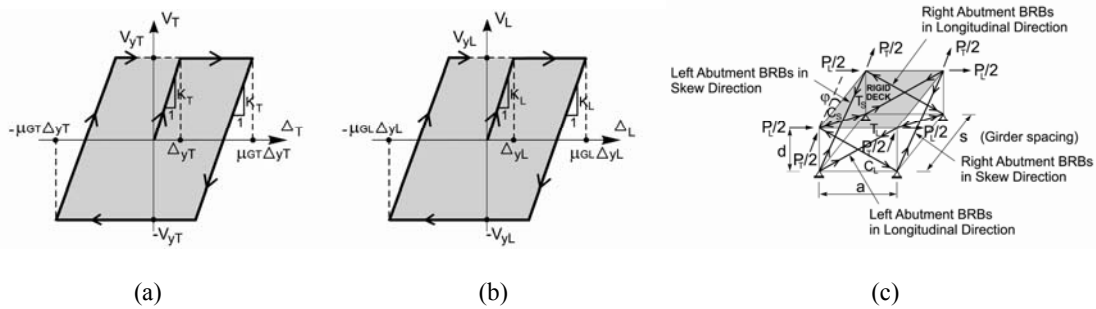


**Figure 2.** (a,b) Transverse and longitudinal base shear versus displacement hysteretic curves for proposed EDSs (c) 3D model showing bidirectional loading and BRBs forces for EDS-1

assumed to be fully flexible about their connection axis. Since the presence of intermediate cross braces does not impact the seismic behavior of these bridges and can be neglected (Zahrai and Bruneau 1998), a simplified structural model to simulate the system behavior is developed (Fig. 2c). For EDS-2, for example, the steps followed to idealize a typical bridge with end diaphragms into a 3D simpler model are given in Fig. 3. Bridge superstructures with damaged bearings (e.g. following an earthquake), neoprene bearings or bidirectional sliding bearings that could be called the “floating span” are considered. Further details and a similar process of idealization steps for EDS-1 are given in Celik and Bruneau (2007).

These analytical models account for general system geometric dimensions such as the skew angle ( $\phi$ ), girder spacing ( $s$ ), end diaphragm depth ( $d$ ) and length to internal diaphragm anchor point ( $a$ ), as well as bidirectional earthquake effects. Results from this study can help select an appropriate value for the parameter “ $a$ .”

## 4. BIDIRECTIONAL PUSHOVER ANALYSIS OF EDS-1

### 4.1. Overview

Nonlinear pushover analysis is adopted in this work. Equal proportions of the total lateral load in a given direction are applied at each corner of the deck.  $P_L$  and  $P_T$  are the lateral earthquake loads acting at the deck level on one diaphragm in the longitudinal ( $L$ ) and transverse ( $T$ ) directions respectively. The bidirectional loading ratio of  $P_L/P_T$  (or  $P_T/P_L$ ) is typically set constant in the pushover analyses. Pushover stops when the prescribed axial displacement ductility level (i.e.  $\mu$ ) of BRBs is reached. Dissipated energy is calculated when the arbitrarily selected BRB ductility limit is reached.

Analytical results of interest include base shear forces at yield, yield displacements or drifts, member versus global (system) ductility relationships, initial stiffness of the end diaphragm system, total or volumetric hysteretic energy dissipations, in both orthogonal bridge directions (as applicable). Static pushover analyses are also carried out on a set of selected end diaphragm configurations using SAP 2000 (CSI, 1998) to validate the analytical equations formulated. Previous studies (e.g. Black et al. 2002) showed that BRBs ductilities (referred to here as “member ductility” and considered to be a local ductility) are typically greater than  $\mu=20$ , which typically corresponds to a drift ratio of 2~3%. Here, an average value of  $\mu=10$  is considered as a target member ductility in developing diagrams. Note that higher ductility demands correspond to larger drifts; the engineer must ensure that such drifts will not damage other substructure and superstructure elements.

### 4.2. Elastic Behavior (EDS-1)

Longitudinal and transverse base shear forces in the elastic range are respectively equal to  $V_L=2P_L$  and  $V_T=2P_T$ , since there are two end diaphragms considered in this model. Static equilibrium gives the following BRBs axial force ratio under bidirectional loading:

$$\frac{C_L}{C_S} = \frac{T_L}{T_S} = \sqrt{\frac{1 + (d/a)^2}{1 + (d/s)^2}} (P_L / P_T \cos \varphi - \sin \varphi) \quad (4.1)$$

where  $T_L$ ,  $C_L$ ,  $T_S$ , and  $C_S$  show tension and compression forces in the longitudinal ( $L$ ) and skew ( $S$ ) BRBs respectively. Depending on the axial force ratios, the possible limit states for this system are as given below:

- If  $\frac{C_L}{C_S} = \frac{T_L}{T_S} < 1$  then the BRBs in the skew direction yield first
- If  $\frac{C_L}{C_S} = \frac{T_L}{T_S} > 1$  then the longitudinal BRBs yield first
- If  $\frac{C_L}{C_S} = \frac{T_L}{T_S} = 1$  then all the BRBs yield at the same time.

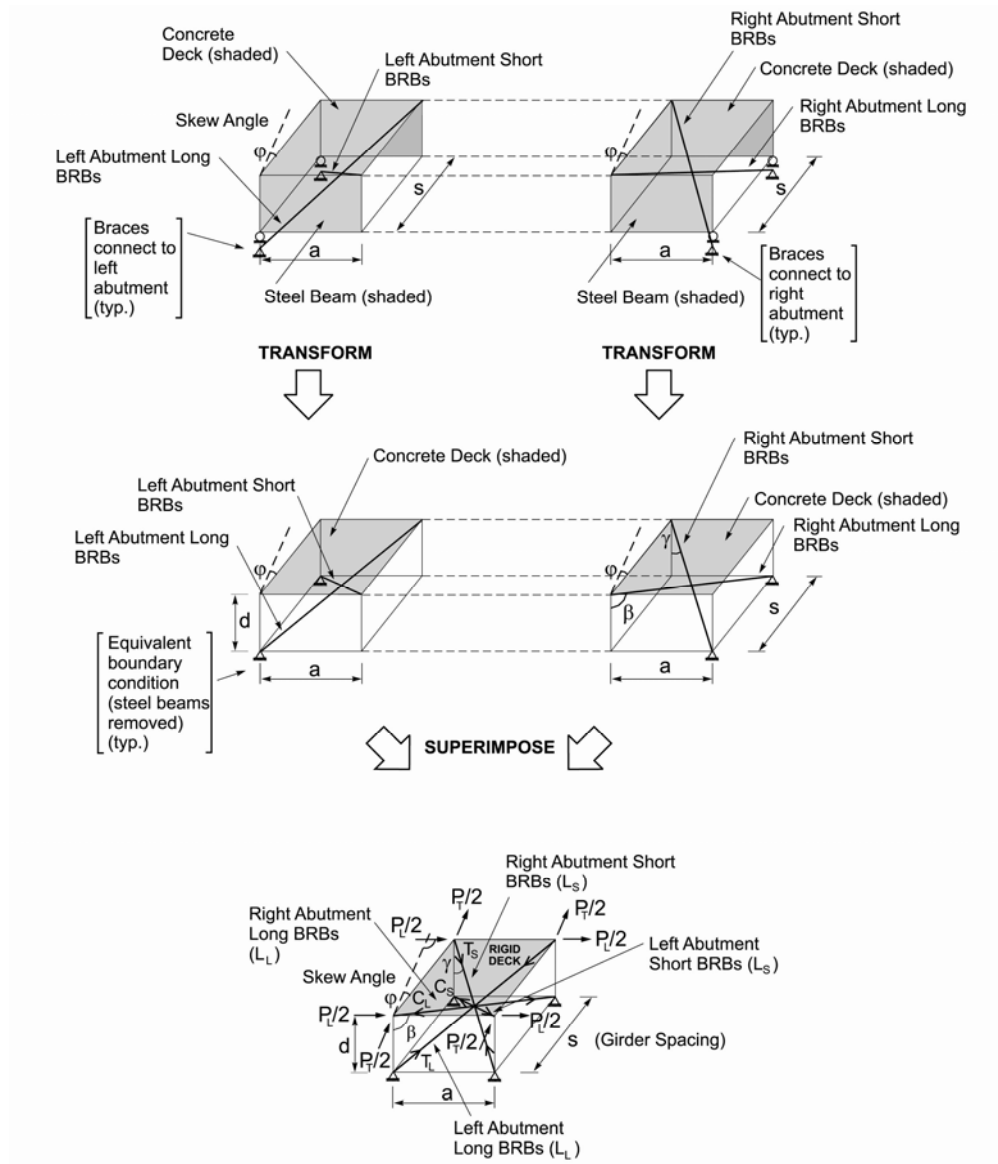


Figure 3. System idealization steps for EDS-2

Numerical values of  $d/s$  of 0.25, 0.50, 1.00, 1.25, and 1.50 as well as values of  $d/a$  equal to 0.20, 0.40, 0.60, 0.80, and 1.00 are considered as proposed by Celik and Bruneau (2007). Since many bridge standards and regulations rely on one of two simplified combination rules to account for bidirectional earthquake effects, here both the 30% rule (AASHTO 2002) and the 40% rule (ATC-32 1996) were considered to show the impact of this value on the behavior of end diaphragm systems.

### 4.3. Inelastic Behavior When Skew BRBs Yield (EDS-1)

Since bridge response is bidirectional due to both bidirectional loading and the skew angle, both transverse and longitudinal responses are investigated for each yielding mechanisms separately.

#### 4.3.1. Transverse response

When  $C_S, T_S > C_L, T_L$ , the skew braces yield only, and base shear strength ( $V_{yT}$ ), yield displacement ( $\Delta_{yT}$ ) and corresponding drift ( $\Delta_{yT}/d$ ) at yield, global ductility ( $\mu_{GT}$ ), and the stiffness of the system ( $K_T$ ) in the transverse direction can be obtained depending on the bridge geometry and BRB properties. Base shear component in the transverse direction ( $V_{yT}$ ) can be calculated as:

$$V_{yT} = \frac{n_S \cos \varphi}{\sqrt{1 + (d/s)^2}} (F_y A) \quad (4.2)$$

where  $F_y$  and  $A$  are the yield stress and cross sectional area of each brace.  $n_S$  and  $n_L$  are the number of BRBs placed in the skew and longitudinal directions respectively. Equal number of BRBs in both directions will be used in this study (i.e.  $n = n_S = n_L$ ). Lateral displacements of the system can be determined using the method of virtual work. Following this procedure gives the lateral drift (i.e.  $\Delta_{yT}/d$ ) in the transverse direction at yielding of the skew BRBs as follows:

$$\frac{\Delta_{yT}}{d} = \frac{[1 + (d/s)^2]^{3/2} (d/a) - [1 + (d/a)^2]^{3/2} (d/s) \sin \varphi (P_L / P_T \cos \varphi - \sin \varphi) \left( \frac{F_y}{E} \right)}{(d/a)(d/s) \sqrt{1 + (d/s)^2} \cos \varphi} \quad (4.3)$$

The ratio of maximum displacement to the yield displacement in the transverse direction (i.e. the system global ductility,  $\mu_{GT}$ ) can be obtained by the ratio of the displacements that correspond to  $\mu=1$  and  $\mu=1$ . Hence,

$$\mu_{GT} = \frac{[1 + (d/s)^2]^{3/2} (d/a) \mu - [1 + (d/a)^2]^{3/2} (d/s) (P_L / P_T \cos \varphi - \sin \varphi) \sin \varphi}{[1 + (d/s)^2]^{3/2} (d/a) - [1 + (d/a)^2]^{3/2} (d/s) (P_L / P_T \cos \varphi - \sin \varphi) \sin \varphi} \quad (4.4)$$

Dividing Eq. (4.2) by Eq. (4.3) gives the initial stiffness ( $K_T$ ) of the system in the transverse direction:

$$K_T = \frac{n (d/s)(d/a) \cos^2 \varphi}{[1 + (d/s)^2]^{3/2} (d/a) - [1 + (d/a)^2]^{3/2} (d/s) (P_L / P_T \cos \varphi - \sin \varphi) \sin \varphi} \left( \frac{EA}{d} \right) \quad (4.5)$$

which enables to evaluate the initial stiffness of the system in terms of axial stiffness of the BRB. Hysteretic energy dissipation ( $E_H$ ) during a complete cycle is given by the shaded area in Fig. 2, or equivalently, the same hysteresis can be calculated from the sum of the hysteretic energy for all individual yielding members. Also, the corresponding hysteretic energy per total brace volume ( $Vol.$ ) is useful for comparison purposes. Performing this calculation gives

$$\frac{E_H}{Vol.} = \frac{4(\mu-1)}{1 + \frac{(d/s)}{(d/a)} \sqrt{1 + (d/a)^2}} \left( \frac{F_y^2}{E} \right) \quad (4.6)$$

#### 4.3.2. Longitudinal response

In a similar manner, base shear, yield drift, and initial stiffness can be calculated for response in the longitudinal direction. The longitudinal component of base shear ( $V_L$ ) when the skew BRBs yield is equal to the following:

$$V_L = \frac{n_s \sin \varphi + n_L (P_L / P_T \cos \varphi - \sin \varphi)}{\sqrt{1 + (d/s)^2}} (F_y A) = \frac{n P_L / P_T \cos \varphi}{\sqrt{1 + (d/s)^2}} (F_y A) \quad (4.7)$$

Using the longitudinal displacement ( $\Delta_L$ ), drift at yielding of skew BRBs can be expressed as

$$\frac{\Delta_L}{d} = \frac{[1 + (d/a)^2]^{3/2} (P_L / P_T \cos \varphi - \sin \varphi)}{(d/a) \sqrt{1 + (d/s)^2}} \left( \frac{F_y}{E} \right) \quad (4.8)$$

Using Eqs. (4.7) and (4.8), initial stiffness in the longitudinal direction can be obtained as

$$K_L = \frac{n (d/a) P_L / P_T \cos \varphi}{[1 + (d/a)^2]^{3/2} (P_L / P_T \cos \varphi - \sin \varphi)} \left( \frac{EA}{d} \right) \quad (4.9)$$

Here, a 345MPa grade steel with  $E=200000$  MPa is assumed for the results presented in Fig.4. Fig. 4a shows the variation of nondimensional transverse base shear as a function of end diaphragm geometric ratios when skew BRBs yield. There is a decrease in this value as the  $d/s$  ratio and skew angle ( $\varphi$ ) increase due to larger direction angles resulting in smaller horizontal force components.

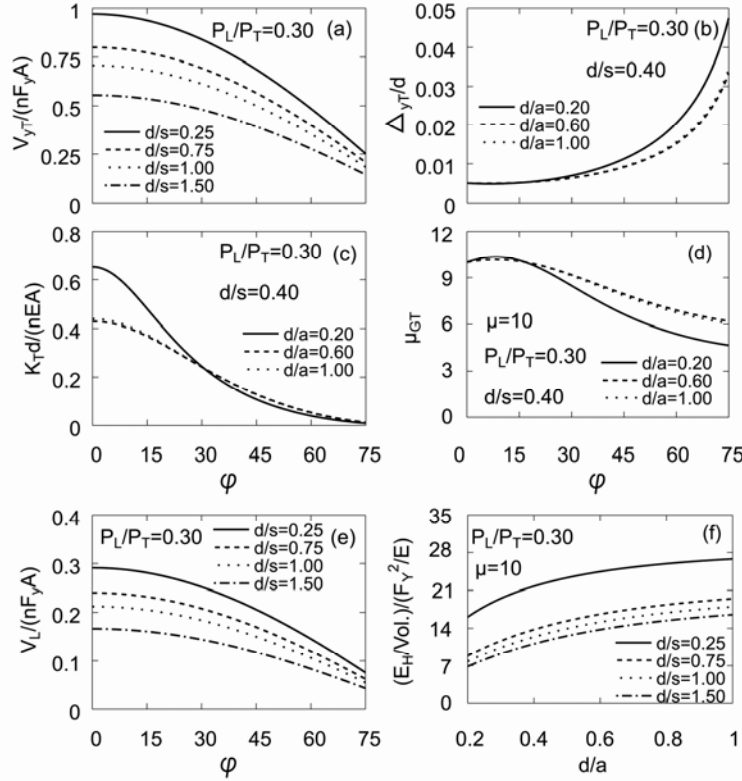


**Figure 4.** Variation of behavioral characteristics when skew BRBs yield: (a) Nondimensional transverse base shear strength versus skew angle ( $\varphi$ ); (b) Transverse yield drift versus  $\varphi$ ; (c) Nondimensional transverse stiffness versus  $\varphi$ ; (d) Global transverse ductility ratio versus  $\varphi$ ; (e) Nondimensional longitudinal base shear versus  $\varphi$ ; (f) Volumetric energy dissipation versus  $d/a$  ratio for  $\mu=10$ .

For  $d/s=0.40$ , transverse drift ( $\Delta_{yT}/d$ ) at yield versus  $\varphi$  is illustrated in Fig. 4b per Eq. (4.3), revealing that drift increases as  $\varphi$  increases. Note that the rate of this increase is more at large skew angles when  $\varphi \geq 30^\circ$ . Variation of nondimensional transverse stiffness is given in Fig. 4c, showing a rapid decrease in stiffness at large skew angles (again when  $\varphi \geq 30^\circ$ ). While the impact of  $d/a$  ratio on drift is more pronounced at large skew angles, stiffness is less affected by this ratio at large skew angles. Global transverse ductility ratio is plotted against  $\varphi$  in Fig. 4d. This ratio is more affected by the  $d/a$  ratio at large skew angles. Nondimensional base shear in the longitudinal direction versus  $\varphi$  is given in Fig. 4e. Similar trends are observed for other behavioral parameters in the longitudinal direction (not presented here due to space constraints). For  $\mu=10$ , Fig. 4f illustrates that nondimensional dissipated hysteretic energy increases as  $d/a$  increases for constant values of  $d/s$  (which could be important in an existing bridge retrofit design), but decreases as  $d/s$  increases for constant values of  $d/a$  (which could be important in a new bridge design). This means that smaller  $d/s$  ratios corresponding to fewer girders (or girders with larger spacing) result in more energy dissipation in the system.

#### 4.4. Inelastic Behavior When Longitudinal BRBs Yield (EDS-1)

Similar formulas are obtained when longitudinal BRBs yield. Derivations and further details are given and discussed in Celik and Bruneau (2007).

### 5. BIDIRECTIONAL PUSHOVER ANALYSIS OF EDS-2

Similar analytical expressions can be developed to describe the behavior of skewed bridges having the EDS-2 configuration of end diaphragms. Special cases are also considered to investigate the effect of certain parameters on the bidirectional seismic response of these bridges. Figs. 1b and 3 show the selected configuration of BRBs for EDS-2. Note that in this case, BRB lengths differ from each other (i.e. the lengths of long ( $L_L$ ) and short ( $L_S$ ) BRBs).

#### 5.1. Elastic Behavior (EDS-2)

To obtain load-displacement diagrams for the system considered, it is convenient to evaluate the ratio of short and long BRBs elastic forces. Using the geometry in Fig. 3, elastic axial force ratio of the BRBs is obtained as follows:

$$\frac{C_L}{C_S} = \frac{T_L}{T_S} = \sqrt{\frac{1+(s/a)^2+(d/a)^2+2(s/a)\sin\varphi}{1+(s/a)^2+(d/a)^2-2(s/a)\sin\varphi}} \left[ \frac{(s/a)(\sin\varphi - P_L/P_T \cos\varphi) - 1}{(s/a)(-\sin\varphi + P_L/P_T \cos\varphi) - 1} \right] \quad (5.1)$$

Here,  $C_S$ ,  $T_S$  and  $C_L$ ,  $T_L$  denote axial compression and tension forces in the short and longitudinal BRBs respectively. In the elastic range, shear forces in each longitudinal and transverse directions are  $V_L=2P_L$  and  $V_T=2P_T$ . The possible limits of the brace force ratio and the corresponding meaning are:

If	$\frac{C_L}{C_S} = \frac{T_L}{T_S} < 1$	then the short BRBs yield first
If	$\frac{C_L}{C_S} = \frac{T_L}{T_S} > 1$	then the long BRBs yield first
If	$\frac{C_L}{C_S} = \frac{T_L}{T_S} = 1$	then all BRBs yield at the same time

#### 5.2. Inelastic Behavior When Short BRBs Yield (EDS-2)

##### 5.2.1. Transverse response

To obtain the yield shear force in the transverse direction when short BRBs yield, the same procedure

followed for EDS-1 is repeated. Writing the equations of equilibrium in the transverse direction gives:

$$V_{yT} = \left[ \frac{4(s/a) \cos \varphi}{\sqrt{1 + (s/a)^2 + (d/a)^2 - 2(s/a) \sin \varphi} [(s/a)(\sin \varphi - P_L/P_T \cos \varphi) + 1]} \right] (F_y A) \quad (5.2)$$

Similarly, the yield drift in the transverse direction can be obtained as

$$\begin{aligned} \frac{\Delta_{yT}}{d} = & \left[ 1 + (s/a)^2 + (d/a)^2 - 2(s/a) \sin \varphi \right]^{3/2} [(s/a) \sin \varphi + 1] [(s/a)(P_L/P_T \cos \varphi - \sin \varphi) - 1] + \\ & \left[ 1 + (s/a)^2 + (d/a)^2 + 2(s/a) \sin \varphi \right]^{3/2} [(s/a)(P_L/P_T \cos \varphi - \sin \varphi) + 1] [(s/a) \sin \varphi - 1] \left( \frac{F_y}{E} \right) / \\ & 2(d/a)(s/a) \sqrt{1 + (s/a)^2 + (d/a)^2 - 2(s/a) \sin \varphi} \cos \varphi [(s/a)(P_L/P_T \cos \varphi - \sin \varphi) - 1] \end{aligned} \quad (5.3)$$

### 5.2.2. Longitudinal response

The following behavioral characteristics are reached for response in the longitudinal direction:

$$V_{yL} = \left[ \frac{4(s/a) P_L/P_T \cos \varphi}{\sqrt{1 + (s/a)^2 + (d/a)^2 - 2(s/a) \sin \varphi} [(s/a)(P_L/P_T \cos \varphi - \sin \varphi) - 1]} \right] (F_y A) \quad (5.4)$$

And, the corresponding drift in the longitudinal direction can be expressed as

$$\begin{aligned} \frac{\Delta_{yL}}{d} = & \left[ 1 + (s/a)^2 + (d/a)^2 - 2(s/a) \sin \varphi \right]^{3/2} [(s/a)(\sin \varphi - P_L/P_T \cos \varphi) + 1] + \\ & \left[ 1 + (s/a)^2 + (d/a)^2 + 2(s/a) \sin \varphi \right]^{3/2} [(s/a)(\sin \varphi - P_L/P_T \cos \varphi) - 1] \left( \frac{F_y}{E} \right) / \\ & 2(d/a) \sqrt{1 + (s/a)^2 + (d/a)^2 - 2(s/a) \sin \varphi} [(s/a)(P_L/P_T \cos \varphi - \sin \varphi) - 1] \end{aligned} \quad (5.5)$$

Initial stiffness of the system in the transverse and longitudinal directions can be obtained from Eqs. (5.2) and (5.3) and Eqs. (5.4) and (5.5) respectively. Since these resulting equations are too long, only numerical results are shown in Fig. 5. Taking  $d/a=0.60$  as constant and  $s/a$  as variable, Fig. 5a shows the nondimensional transverse base shear strength as a function of the skew angle ( $\varphi$ ). For constant values of  $s/a$ , a decrease in the nondimensional base shear is observed as  $\varphi$  increases. The  $s/a$  ratio has an important impact on the base shear at smaller skew angles. For constant values of  $\varphi$ , the base shear strength decreases as  $s/a$  decreases. As shown in Fig. 5b, the transverse yield drift ( $\Delta_{yT}/d$ ) increases as  $\varphi$  increases, but decreases as  $s/a$  increases, revealing that BRBs with larger direction angles would be preferable to obtain stiffer end diaphragms. This also suggests that EDS-2 is more effective when sufficient girder spacing exists in the bridge superstructure. As expected, the increase in drift is less at smaller skew angles when  $\varphi \leq 30^\circ$ , suggesting severely skewed systems should be avoided if possible. From Fig. 5c, the nondimensional transverse stiffness is observed to decrease as  $\varphi$  increases for the most ratios of  $s/a$ . Fig. 5d gives the variation of longitudinal base shear versus  $\varphi$ , revealing a decrease in this value with increasing skew angle. For smaller values of  $s/a$  ratio, Fig. 5e illustrates that there is an increase in the longitudinal drift ( $\Delta_{yL}/d$ ). Comparing transverse and longitudinal drift diagrams shows that although relatively larger drifts are obtained in the transverse direction for small  $s/a$  ratios, both transverse and longitudinal drifts are much closer to each other especially for larger  $\varphi$  angles. As seen in Fig. 5f, longitudinal stiffness decreases as  $\varphi$  increases for the most practical values of  $s/a$ . For a wide range of skew angles, comparing transverse and longitudinal stiffnesses gives that the stiffness in the longitudinal direction is larger than the transverse stiffness for smaller values of  $s/a$ . As  $\varphi$  and  $s/a$  increase, closer stiffnesses are obtained in both directions.

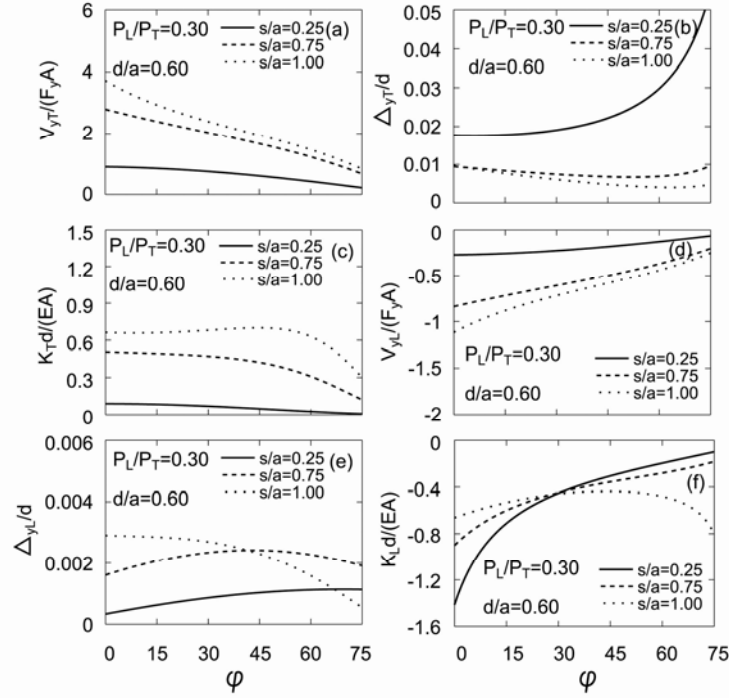


**Figure 5.** Variation of behavioral characteristics when short BRBs yield: (a) Nondimensional transverse base shear strength versus skew angle ( $\varphi$ ); (b) Transverse yield drift versus  $\varphi$ ; (c) Nondimensional transverse stiffness versus  $\varphi$ ; (d) Nondimensional longitudinal base shear strength versus  $\varphi$ ; (e) Nondimensional longitudinal yield drift versus  $\varphi$ ; (f) Nondimensional longitudinal stiffness versus  $\varphi$ .

### 5.2.3. Hysteretic energy dissipation

The dissipated volumetric energy in this case can be given as follows:

$$\frac{E_H}{Vol.} = \frac{4(\mu-1)\sqrt{1+(s/a)^2+(d/a)^2}-2(s/a)\sin\varphi}{\sqrt{1+(s/a)^2+(d/a)^2}-2(s/a)\sin\varphi + \sqrt{1+(s/a)^2+(d/a)^2}+2(s/a)\sin\varphi} \left( \frac{F_y^2}{E} \right) \quad (5.6)$$

Assuming  $d/a=0.60$ ,  $\mu=10$  and as depicted in Figs. 6a and 6b, hysteretic energy decreases as  $\varphi$  increases. Changes in the  $s/a$  ratio have more effect on the dissipated energy at larger  $\varphi$  angles. Compared to  $d/a=0.60$ , the end diaphragm system with  $d/a=1.00$  dissipates more energy at larger  $\varphi$  angles.

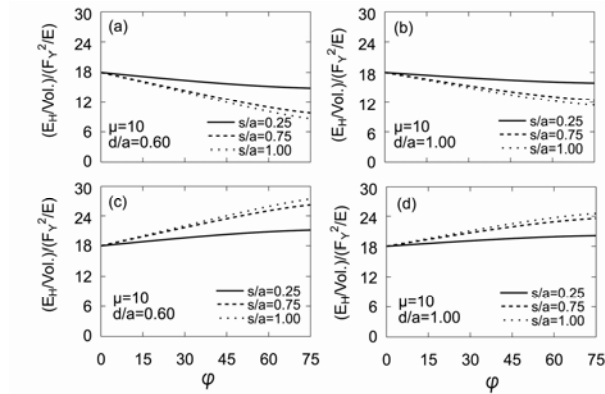


**Figure 6.** Variation of volumetric energy dissipation with  $\varphi$  (For  $\mu=10$ ): (a) Short BRBs yield and  $d/a=0.60$ ; (b) Short BRBs yield and  $d/a=1.00$ ; (c) Long BRBs yield and  $d/a=0.60$ ; (d) Long BRBs yield and  $d/a=1.00$ .

### 5.3. Inelastic Behavior When Long BRBs Yield (EDS-2)

Derivations of formulas and further details are given and discussed in Celik and Bruneau (2007).

## 6. CONCLUSIONS

The major conclusions reached from this study are as follows:

1. Skewness has a more severe impact on the end diaphragms seismic behavior, although not a significant one until  $\phi \geq 30^\circ$ . While the base shear strength and lateral stiffness decrease as the skew angle increases, drifts increase instead.
2. For EDS-1, smaller drifts are obtained in skewed bridges for larger  $d/a$  values and do not change much after  $d/a = 1.00$ . Also, dissipated energy per BRB volume used is less affected after  $d/s=1.00$ . These suggest that appropriate values for both  $d/a$  and  $d/s$  ratios could be selected between 0.5 and 1.0. A similar observation is made for EDS-2, as larger  $s/a$  ratios have a less impact on the behavioral characteristics (e.g. base shear, drift, stiffness as well as the dissipated energy), appropriate values for the  $s/a$  ratio could also be selected between 0.5 and 1.0. Severely skewed systems had a poorer response and should be avoided if possible.
3. Some of the assumptions made in this paper could be eliminated in future analytical work. For example, diaphragms having BRBs of unequal area (if deemed to be useful in some applications) could be investigated.

## ACKNOWLEDGMENTS

This research was conducted by the State University of New York (SUNY) at Buffalo and was supported by the Federal Highway Administration (FHWA) under contract number DTFH61-98-C-00094 to the Multidisciplinary Center for Earthquake Engineering Research (MCEER).

## REFERENCES

- AASHTO. (2002). Standard Specifications for Highway Bridges. Washington, D.C.
- AASHTO. (2009). Guide Specifications for LRFD Seismic Bridge Design. Washington, D.C.
- ATC-32. (1996). Improved Seismic Design Criteria for California Bridges: Provisional Recommendations. California-Washington, D.C.
- Black, C., Makris, N. and Aiken, I. (2002). Component Testing, Stability Analysis and Characterization of Buckling-Restrained Unbonded Braces. PEER Report-2002/08. Pacific Earthquake Engineering Research Center. University of California, Berkeley.
- Carden, L.P., Itani, A.M. and Buckle, I.G. (2006). Seismic performance of steel girder bridges with ductile cross frames using buckling-restrained braces. *J. Struct. Eng.-ASCE*. **132:3**, 338-345.
- Celik, O.C. and Bruneau, M. (2007). Seismic Behavior of Bidirectional-Resistant Ductile End Diaphragms with Unbonded Braces in Straight or Skewed Steel Bridges. Technical Report, MCEER-07-0003. MCEER-Earthquake Engineering to Extreme Events, Buffalo, NY.
- Computers and Structures, Inc., CSI. (1998). SAP2000 Integrated Finite Element Analysis and Design of Structures-Detailed Tutorial including Pushover Analysis. Berkeley, CA.
- Kanaji H., Kitazawa, M. and Suzuki, N. (2003). Seismic Retrofit Strategy using Damage Control Design Concept and the Response Reduction Effect for a Long-Span Truss Bridge. *19th US-Japan Bridge Eng. Workshop-Panel on Wind and Seismic Effects, UJNR*. Tsukuba Science City, Japan.
- Lopez, W. and Sabelli, R. (2004). Seismic Design of Buckling-Restrained Braced Frames. Steel Tips. The Structural Steel Educational Council, Moraga, CA.
- Zahrai, S.M. and Bruneau, M. (1998). Impact of diaphragms on seismic response of straight slab-on-girder steel bridges. *J. Struct. Eng.-ASCE*. **124:8**, 938-947.
- Zahrai, S.M. and Bruneau, M. (1999a). Ductile end-diaphragms for seismic retrofit of slab-on-girder steel bridges. *J. Struct. Eng.-ASCE*. **125:1**, 71-80.
- Zahrai, S.M. and Bruneau, M. (1999b). Cyclic testing of ductile end-diaphragms for slab-on-girder steel bridges. *J. Struct. Eng.-ASCE*. **125:9**, 987-996.